Proceedings of OMAE 2005:
24th International Conference on Offshore Mechanics and Arctic Engineering
Halkidiki, Greece, 12-17 June 2005

OMAE2005-67355

CFD INVESTIGATION OF THE EFFECT OF CURRENT TURBULENCE ON THE HYDRODYNAMIC FORCES ON A CYLINDER

Hyung Taek Ahn
Offshore Technology Research Center and
The University of Texas at Austin

Yannis Kallinderis
Offshore Technology Research Center

ABSTRACT

Practical cases of flow-structure interactions involve ocean currents with turbulence. Ocean turbulence effects on offshore structures are of high interest due to the lack of information about its role regarding the hydrodynamic forces and fatigue load on structures. Current turbulence profiles are employed for various Reynolds numbers that are based on an isotropic geophysical turbulence model. These turbulence profiles are specified as the inflow condition for the numerical simulations over a circular cylinder. The present work consists of three parts: (i) determination of appropriate mesh and time step resolution to accommodate the turbulence, (ii) investigation of the effect of current profile turbulence on the amplitude and frequencies of the hydrodynamic forces acting on a cylinder, and (iii) study of the sensitivity of the hydrodynamic load exerted on the cylinder for a range of Reynolds numbers with a turbulent inflow profile. Spalart-Allmaras one-equation turbulence model is used for high Reynolds number simulations.

INTRODUCTION

Turbulent flows are present everywhere. Especially, the inflow ocean turbulent effects on offshore structures are of high interest due to the lack of information about its role regarding the hydrodynamic forces and fatigue load on structures.

Two different inflow turbulence profiles are employed that are based on an isotropic geophysical turbulence model [1]. One for low Reynolds number flows as shown in Fig. 1 and the other is used for high Reynolds number flows as displayed in Fig. 2. These turbulence profiles are specified as the inflow condition for the current numerical simulations over a circular cylinder, our representative offshore structure. In order to study free stream turbulence effects on the flows around a cylinder, a turbulent velocity profile is to be prescribed at the inlet instead of the uniform velocity profile. The 2D turbulent velocity profile is a slice of the 3D turbulence profile employed [1].

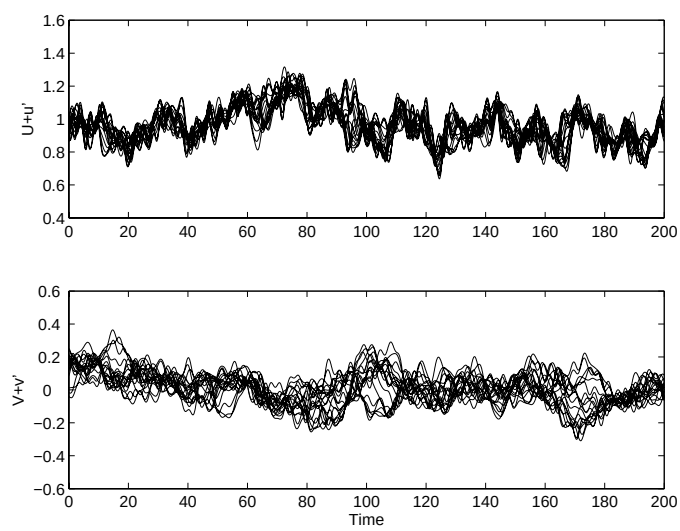

Fig. 1. Inflow turbulent velocity profiles used for low Reynolds number (Re=150) inflow turbulent flow simulation. The average velocity fluctuations at the inlet are $\hat{u} = \sqrt{\overline{(u')^2}} \Big/ U_\infty = 0.1115$ and $\hat{v} = \sqrt{\overline{(v')^2}} \Big/ U_\infty = 0.1115$.

Copyright © #### by ASME

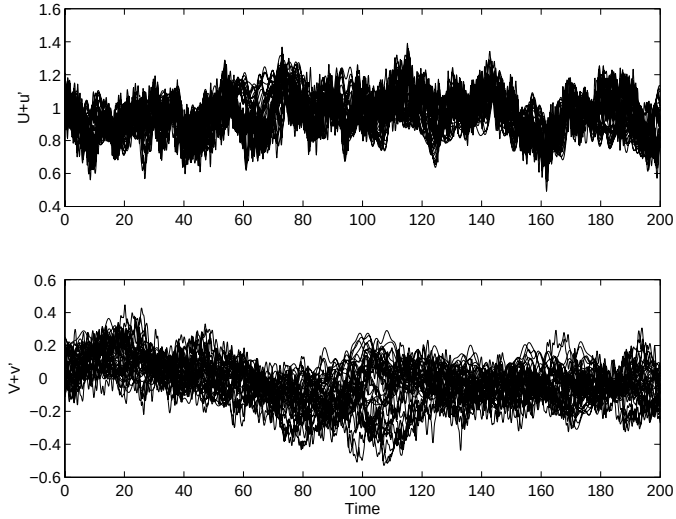

Fig. 2. Inflow turbulent velocity profiles used for high Reynolds number (Re ≥ 1,000) inflow turbulent flow simulations. The average velocity fluctuations at the inlet are $\hat{u} = \sqrt{\overline{(u')^2}} \Big/ U_\infty = 0.1297$ and $\hat{v} = \sqrt{\overline{(v')^2}} \Big/ U_\infty = 0.1449$.

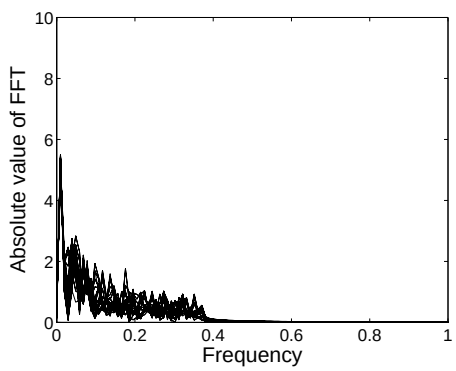

(a) u'

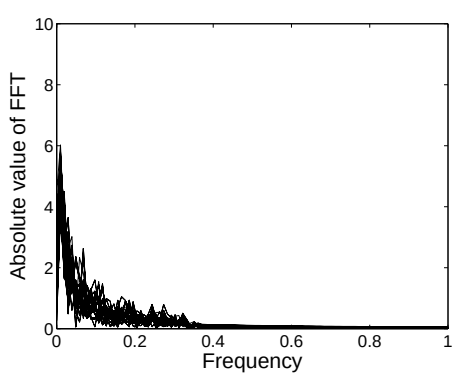

(b) v'

Fig. 3. FFT spectrum of inflow turbulence fluctuations as shown in Fig. 1.

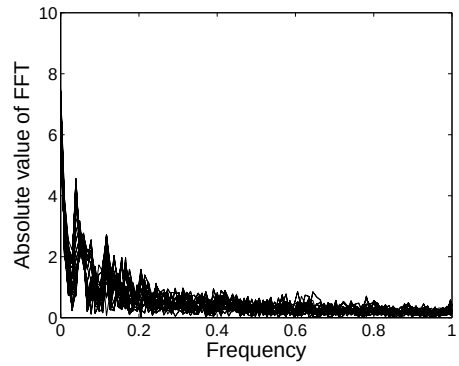

(a) u'

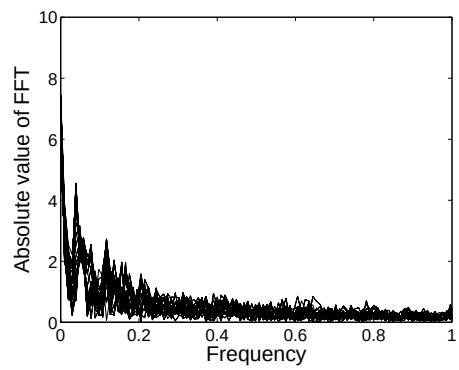

(b) v'

Fig. 4. FFT spectrum of inflow turbulence fluctuations, as shown in Fig. 2.

Comparing the two inlet turbulent profiles ($u = U + u'$, $v = V + v'$) displayed in Fig. 1 and in Fig. 2, it is evident that the second profile is characterized by higher amplitude and higher frequencies of the fluctuations and also wider spatial variations of the fluctuations. In Fig. 3 and 4, the FFT spectra of the inflow turbulences, which are shown in Fig. 1 and 2, are displayed. The higher frequencies in the inflow turbulence fluctuations are observed in Fig. 4 compared to the Fig. 3.

Time step and mesh convergence studies for various Reynolds numbers determined the appropriate time and space scales which are suitable for resolution of the current profile turbulence, as well as its evolution downstream. The determination was based on monitoring of the changes in the predicted hydrodynamic forces with refinement of the time step and mesh.

The Reynolds-averaged Navier-Stokes method with the special boundary conditions and scales for treatment of the turbulence is applied to prediction of the hydrodynamic forces acting on a cylinder for various Reynolds numbers. Spalart-

Copyright © #### by ASME

Allmaras one-equation eddy-viscosity model [7] is used for high Reynolds number simulations. All cases of current profile turbulence are also compared to their corresponding uniform current cases in terms of the amplitudes and frequencies of the forces. The range of Reynolds numbers considered is from low subcritical to supercritical numbers.

NUMERICAL METHOD

The incompressible Navier-Stokes equations are written in terms of mass and momentum conservation. The time accurate formulation of the artificial compressibility method is employed. The conservation laws of mass and momentum for an arbitrarily closed control volume V with the boundary S in integral form can be expressed as

$$\frac{d}{dt}\int_V \rho dV + \int_S \rho\left(\mathbf{V}-\mathbf{V}_b\right)\cdot\hat{\mathbf{n}}dS = 0 \qquad (1)$$

$$\frac{d}{dt}\int_V \rho\mathbf{V}dV + \int_S \rho\mathbf{V}\left(\mathbf{V}-\mathbf{V}_b\right)\cdot\hat{\mathbf{n}}dS = \int_S \boldsymbol{\sigma}\cdot\hat{\mathbf{n}}dS \qquad (2)$$

where $\mathbf{V}$ is the velocity of the fluid and $\mathbf{V}_b$ is the velocity of the control volume boundary. The stress tensor $\boldsymbol{\sigma}$ is composed of the normal stress representing hydrostatic pressure and the shear stress. The conservation laws, which are nondimensionalized by using the reference quantities of free stream velocity U_∞ and cylinder diameter D, can be expressed in a system as follows

$$\frac{d}{dt}\int_V \mathbf{U}dV + \int_S \left(\mathbf{F}_I\hat{\mathbf{i}}+\mathbf{G}_I\hat{\mathbf{j}}+\mathbf{H}_I\hat{\mathbf{k}}\right)\cdot\hat{\mathbf{n}}dS = \int_S \left(\mathbf{F}_V\hat{\mathbf{i}}+\mathbf{G}_V\hat{\mathbf{j}}+\mathbf{H}_V\hat{\mathbf{k}}\right)\cdot\hat{\mathbf{n}}dS \qquad (3)$$

where each of the vector are defined as below

$$\mathbf{U} = \begin{bmatrix}1 & u & v & w\end{bmatrix}^T$$

$$\mathbf{F}_I = \begin{bmatrix}(u-u_b) & u(u-u_b)+p & v(u-u_b) & w(u-u_b)\end{bmatrix}^T,$$

$$\mathbf{G}_I = \begin{bmatrix}(v-v_b) & u(v-v_b) & v(v-v_b)+p & w(v-v_b)\end{bmatrix}^T,$$

$$\mathbf{H}_I = \begin{bmatrix}(w-w_b) & u(w-w_b) & v(w-w_b) & w(w-w_b)+p\end{bmatrix}^T$$

$$\mathbf{F}_V = \frac{1}{\mathrm{Re}}\begin{bmatrix}0 & 2\frac{\partial u}{\partial x} & \frac{\partial u}{\partial y}+\frac{\partial v}{\partial x} & \frac{\partial u}{\partial z}+\frac{\partial w}{\partial x}\end{bmatrix}^T,$$

$$\mathbf{G}_V = \frac{1}{\mathrm{Re}}\begin{bmatrix}0 & \frac{\partial v}{\partial x}+\frac{\partial u}{\partial y} & 2\frac{\partial v}{\partial y} & \frac{\partial v}{\partial z}+\frac{\partial w}{\partial y}\end{bmatrix}^T,$$

$$\mathbf{H}_V = \frac{1}{\mathrm{Re}}\begin{bmatrix}0 & \frac{\partial w}{\partial x}+\frac{\partial u}{\partial z} & \frac{\partial w}{\partial y}+\frac{\partial v}{\partial z} & 2\frac{\partial w}{\partial z}\end{bmatrix}^T$$

where $\mathbf{U}$ is the vector containing the conserved variables, $\mathbf{F}_I$, $\mathbf{G}_I$, and $\mathbf{H}_I$ are the vectors representing convective fluxes, $\mathbf{F}_V$, $\mathbf{G}_V$, and $\mathbf{H}_V$ are the vectors representing viscous fluxes, and $\mathrm{Re} = \rho U_\infty D/\mu$ is the Reynolds number. Since the conservation laws are nondimensionalized, the boundary conditions, domain size, or cylinder diameter does not change with respect to the Reynolds numbers used, and any change of Reynolds number is directly accounted by the Reynolds number in the viscous flux terms.

The artificial compressibility method [2] is used in a time-accurate formulation. The time advancement scheme of the current formulation requires the dual time-stepping scheme [3,4], which is solving a steady-state problem in pseudo time t^* as follows

$$\frac{d}{dt^*}\left(\mathbf{Q}V\right) + \mathbf{P}^{-1}\mathbf{R}^*\left(\mathbf{Q}\right) = 0 \qquad (4)$$

where $\mathbf{Q}$ is the vector containing unknown flow variables (pressure and velocity components) and $\mathbf{P}$ is the preconditioning matrix containing the artificial compressibility parameter β, and those are defined as follows

$$\mathbf{Q} = \begin{Bmatrix}p\\u\\v\\w\end{Bmatrix}, \qquad \mathbf{P} = \begin{bmatrix}1/\beta & 0 & 0 & 0\\0 & 1 & 0 & 0\\0 & 0 & 1 & 0\\0 & 0 & 0 & 1\end{bmatrix}$$

and $\mathbf{R}^*$ is the unsteady residual which consists of true time evolution terms and convective and viscous fluxes as expressed in Eq. (3). The above steady state problem in pseudo-time t^* is solved iteratively by using a 5-stage multi-stage scheme [4]. Once the steady state in pseudo time is arrived, the pseudo time derivative term in Eq. (4) vanishes and the original incompressible Navier-Stokes equations as expressed in Eq. (3) are recovered.

MESH AND TIME STEP RESOLUTION EFFECTS ON INFLOW TURBULENCE SIMULATIONS

Since the local mesh spacing determines the smallest scale of turbulence fluctuations which can be resolved, adequate mesh resolution has to be assured for accurate simulation of inflow turbulence.

Copyright © #### by ASME

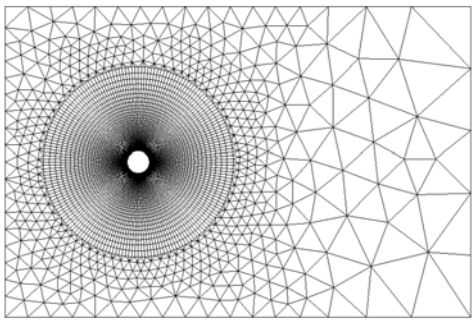

Fig. 5. Original 2D hybrid mesh (13,086 nodes).

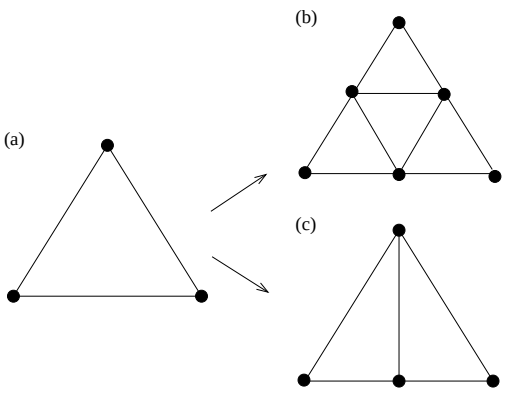

Fig. 6. Division types for triangular elements. (a) original cell, (b) isotropic division, and (c) anisotropic division used only at the transitional regions between the triangular and quadrilateral elements.

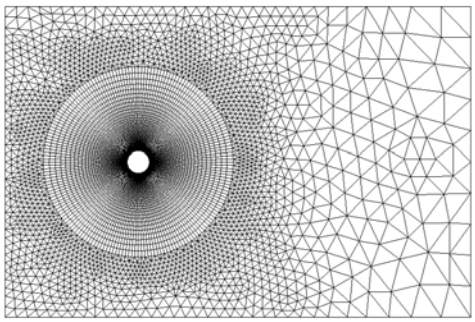

Fig. 7. Locally refined 2D hybrid mesh (14,412 nodes).

For the low Reynolds number case (Re=150), the cylinder diameter is about 10 times smaller than the integral length scale of the upstream turbulence, which is a length scale characterizing coherence of the fluctuations [1,5]. For this case, grid spacing at the inlet boundary is smaller than the cylinder diameter, so the resolution of the computational grid is deemed to be fine enough to capture the smallest eddies.

For higher Reynolds number case (Re=1,000), the scales of the upstream turbulent eddies are smaller, so the computational grid near may need to be refined in order to resolve these smaller scales of eddies.

Two levels of 2D hybrid meshes are employed for the mesh resolution effect study. Based on the original mesh as displayed in Fig. 5, the outer region of triangular cells are refined by using the division types [6] as delineated in Fig. 6. The original mesh of Fig. 5 has been found to be adequate for uniform inflow cases. Since the mesh resolution near the cylinder is already fine enough, only the cells in the upstream and wake regions are refined as shown in Fig. 7, so that the inflow turbulence and its convection downstream can be resolved more accurately.

Copyright © #### by ASME

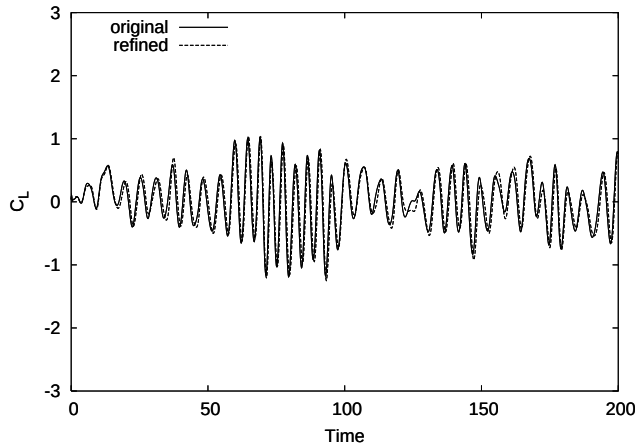

Fig. 8. Mesh adaptation effect on C_L responses (Re=150). Solid lines are for original mesh, and dashed lines are for adapted mesh, which are almost identical.

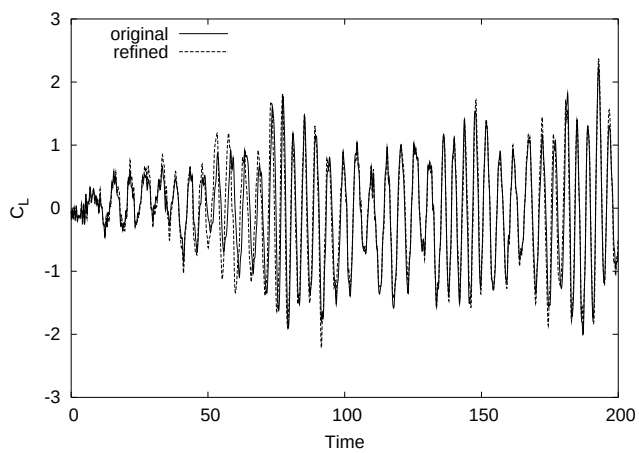

Fig. 9. Mesh adaptation effect on C_L responses (Re=1,000). Solid lines are for original mesh, and dashed lines are for adapted mesh. Extra frequencies are observed for the adapted mesh case.

The mesh refinement effect on the C_L responses is presented in Fig . 8 for Re=150 and in Fig. 9 for Re=1,000. For Re=150, the adapted mesh simulation shows almost identical result to the original mesh simulation. This tells that the original mesh is fine enough to resolve most of the inflow turbulent eddies which are significant to the drag and lift response of the structure. In contrast, for Re = 1,000, there is a noticeable difference in the drag and lift responses between the adapted and original mesh results. Especially, in the fluctuations of the drag and lift coefficients, more frequencies are encountered by the adapted meshes than the original mesh. These extra frequencies in the drag and lift seem to be the direct effect of the smaller scales of eddies which are resolved by the refined mesh. The vorticity fields at the same time are presented in Fig. 10 for the original mesh simulation and in Fig. 11 for the adapted mesh simulation. It is evident that the adapted mesh resolves much smaller scales of eddies transported from the inlet.

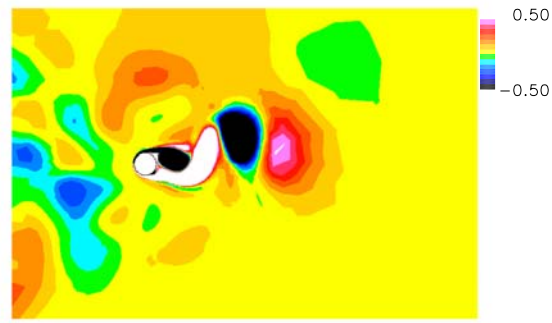

Fig. 10. Vorticity filed obtained from the original mesh simulation (Re=1,000).

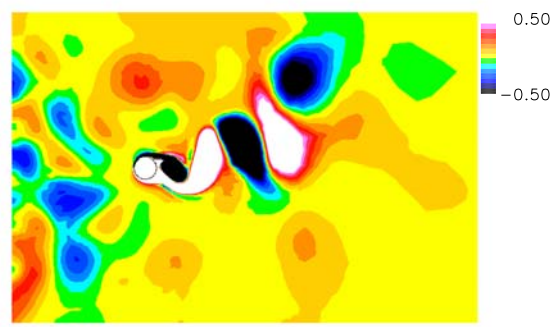

Fig. 11. Vorticity field obtained from the adapted mesh simulation (Re=1,000).

The frequency of the hydrodynamic forces is also important as it is directly related to the fatigue of the structure. Frequency responses to inflow turbulence are presented here. In general, the inflow turbulence introduces more frequencies in vortex shedding and they are spread in wider ranges around the shedding frequency of the uniform inflow case. The details of the frequency analysis are presented in Fig. 12 for Re=150 and Fig. 13 for Re=1,000.

Copyright © #### by ASME

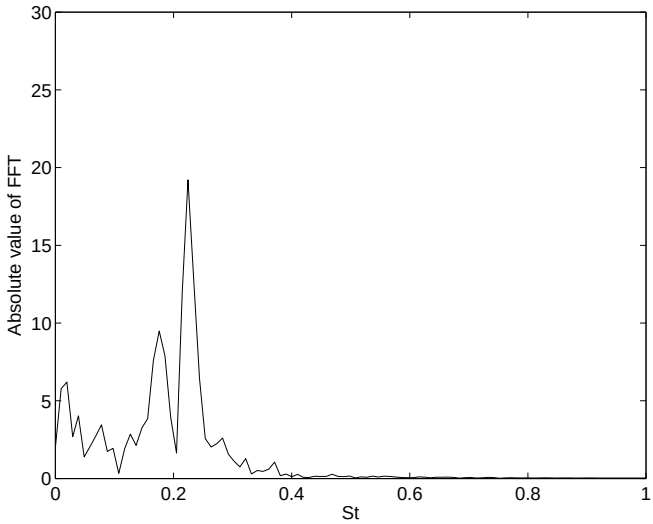

(a) original mesh

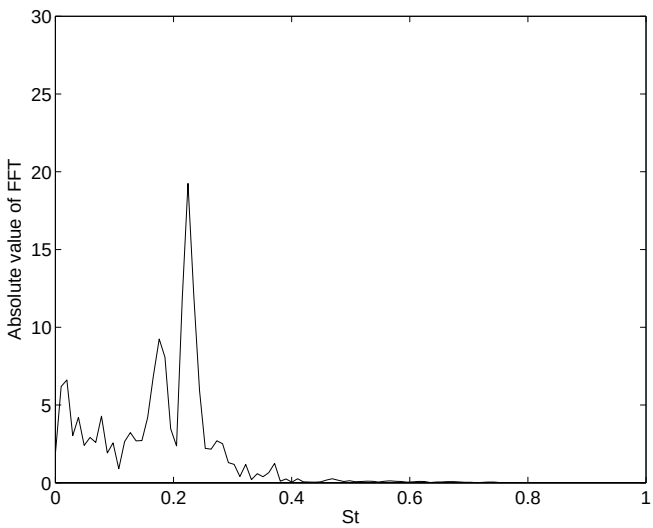

(b) refined mesh

Fig. 12. FFT spectrum of C_L responses (Re=150). Two major frequencies (around $St = 0.2$) are resolved for both of the cases.

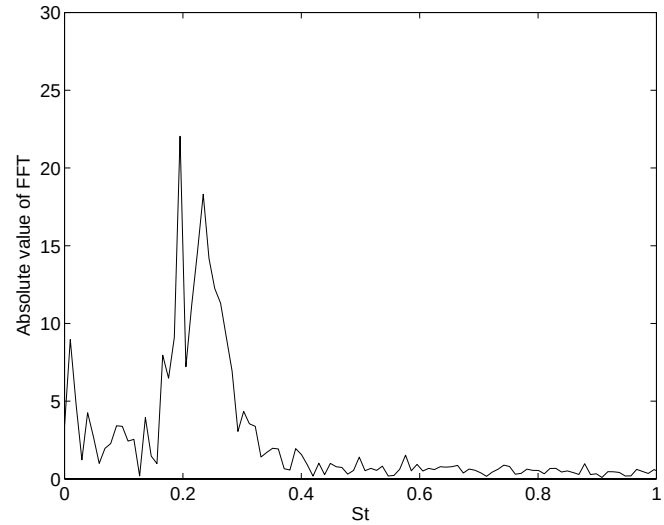

(a) original mesh

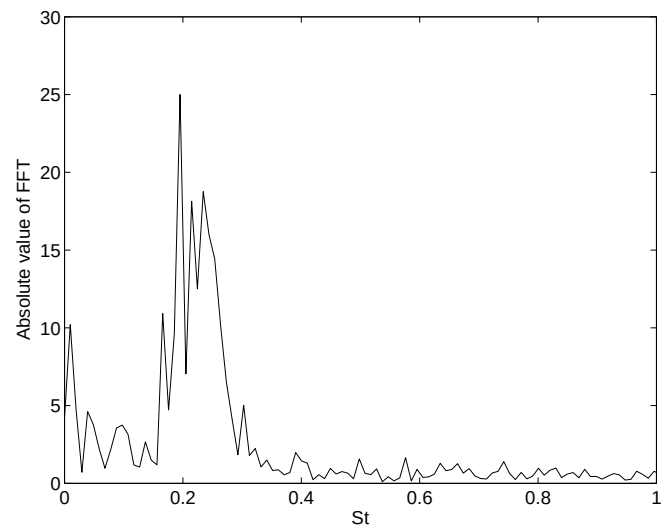

(b) refined mesh

Fig. 13. FFT spectrum of C_L responses (Re=1,000). Additional frequencies (around $St = 0.2$) are resolved by refined mesh simulation.

For the Re=150 case, the frequency responses are almost the same and insensitive to mesh refinement, which means that the original mesh resolves most of the eddies which are significant to the vortex shedding. However, for the Re=1,000 case, the frequency analysis of the adapted mesh simulation reveals more frequencies (four peaks around $St = 0.2$) which were not resolved by the original mesh simulation. This indicates that the refined mesh is resolving more small scales of turbulent eddies and these small eddies result directly in the extra frequencies of shedding.

Finally, the time step size required for the simulation of turbulent flow is investigated. In order to determine the necessary time step size to accommodate turbulence disturbances, a uniform inflow case with initial disturbance is employed and the effect of the initial disturbance is carefully observed. A disturbance is applied by rotating the cylinder during an initial stage of simulation for Re=100,000.

Copyright © #### by ASME

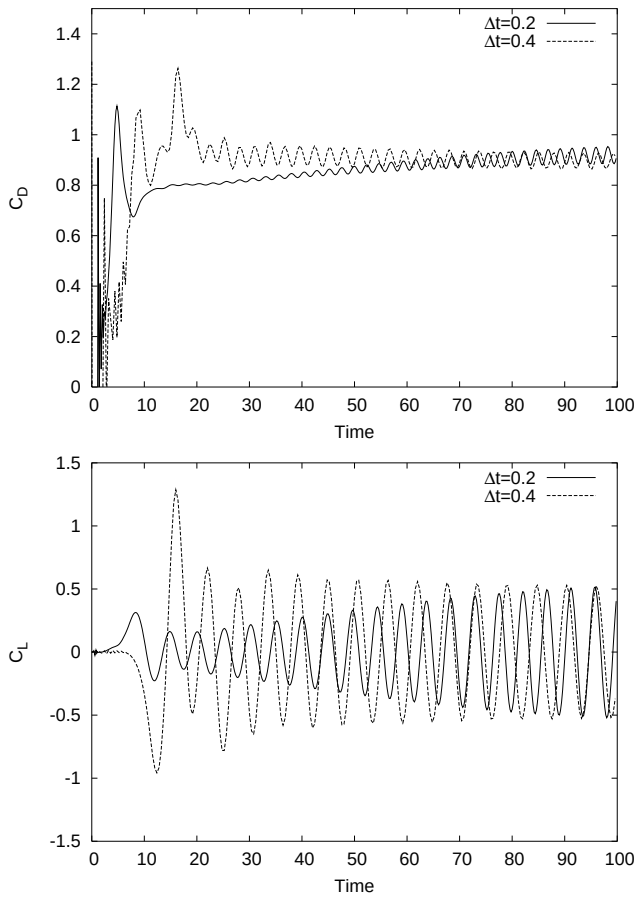

Fig. 14. Time step resolution effect on the decay of initial disturbance (Re=100,000). As time step becomes large ($\Delta t = 0.4$), the initial disturbance persists long and destroy the unsteady solution behavior.

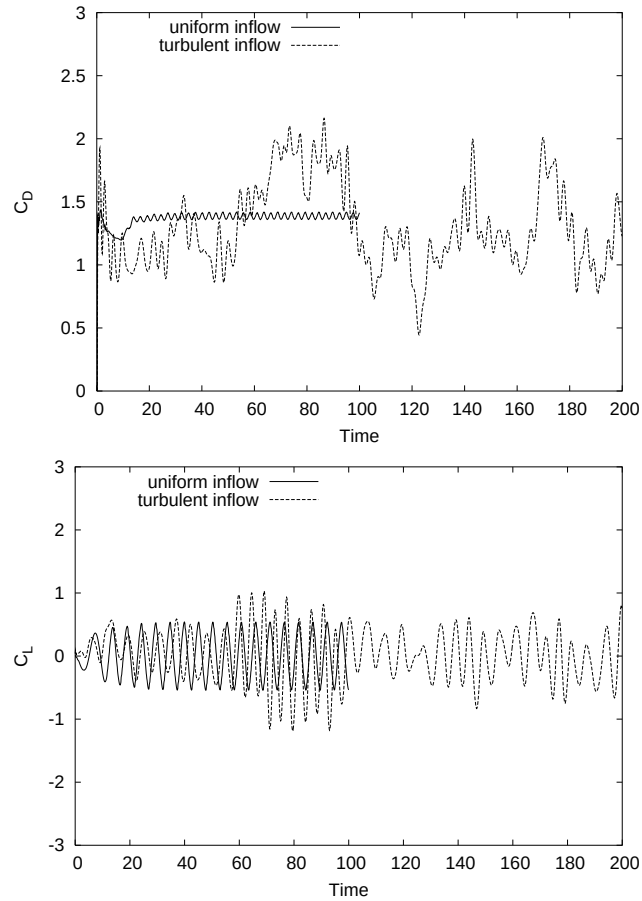

Fig. 15. C_D and C_L responses corresponding to the turbulent and uniform inflow (Re=150). Solid lines are for the uniform inflow, and dashed lines are for the turbulent inflow.

As shown in Fig. 14, excessive fluctuations of C_D and C_L are observed when the time step of $\Delta t = 0.4$ is used. This is because the initial disturbance persists for very long and it affects the overall response of hydrodynamic forces. For the time step $\Delta t = 0.2$, the effect of the disturbance is limited to the initial stage, and does not corrupt the time-accurate solution further. Hence, in order to resolve turbulent fluctuation accurately, all the simulation results are produced with $\Delta t = 0.1$ in this work.

COMPARISON BETWEEN TURBULENT INFLOW AND UNIFORM INFLOW

The effect of the turbulent inflow is further clarified with the comparisons with uniform inflow cases. The hydrodynamic forces exerted on the cylinder with turbulent inflow are presented in Fig. 15 for Re=150 and Fig. 16 for Re=1,000, and they are compared with those of the uniform inflow case.

For both of the cases, the inflow turbulence increases the amplitudes of C_L, magnitudes of C_D, and shedding frequency St. This tendency can be further generalized by a comparison between the inflow turbulence profiles depicted in Fig.'s 1-2 (cause) and the hydrodynamic responses shown in Fig.'s 15-16 (effect). First of all, when the inflow turbulence is applied, *the time series of the drag (in-line force) coefficient usually (not always) follows the time series of the inflow u-velocity*. Furthermore, higher values of C_D are always accompanied with higher amplitudes of C_L as well as faster shedding frequencies. However, there is an exception which does not follow this trend. Especially, in the region of time t=100 to t=120 for Re=1,000, both the C_D and the amplitudes of the C_L decrease even though the inflow u-velocity increases. In that period of time (t=100~120), a large variation of inflow v-velocity is observed in the inflow turbulence profile, and its effect is uncertain at this time and is of interest for further investigation.

Copyright © #### by ASME

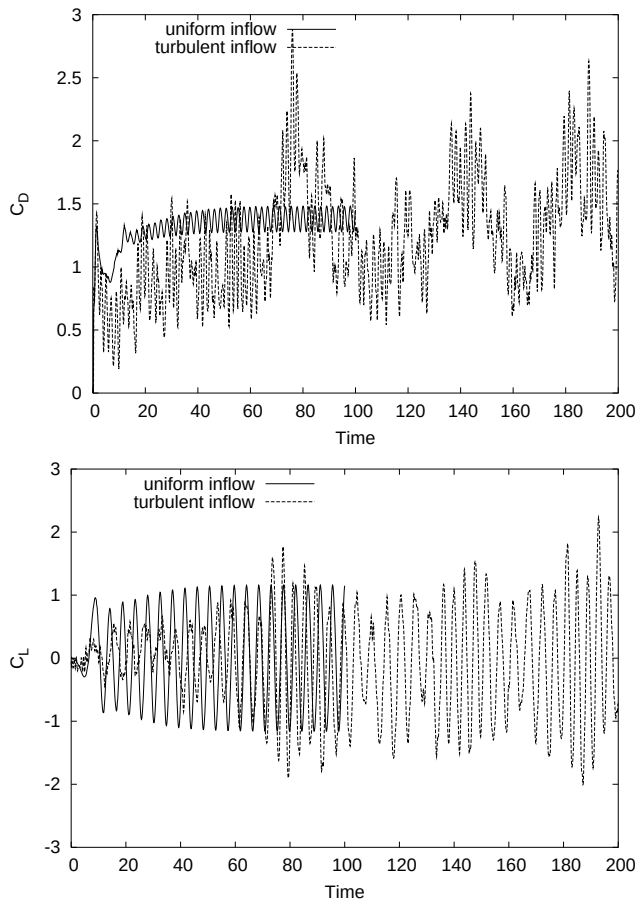

Fig. 16. C_D and C_L responses corresponding to the turbulent and uniform inflow (Re=1,000). Solid lines are for the uniform inflow, and dashed lines are for the turbulent inflow.

The general trends of the drag and lift coefficient to the inflow turbulence profile can be summarized as below.

(i) the stronger the inflow u-velocity fluctuation, the higher the C_D (the higher in-line force).

(ii) the higher C_D accompanies the higher values of peak C_L and St.

HIGH REYNOLDS NUMBER FLOWS WITH INFLOW TURBULENCE

In this section, the effect of Reynolds number for a given turbulent profile is presented. The inflow turbulent profile as shown in Fig. 2 is applied for a series of higher Reynolds number flows, and the hydrodynamic force responses are compared in Fig. 17. For high Reynolds number flow simulations, Spalart-Allmaras one-equation eddy-viscosity model [7] is used. No trip function is used and the eddy-viscosity on the cylinder surface is set to zero.

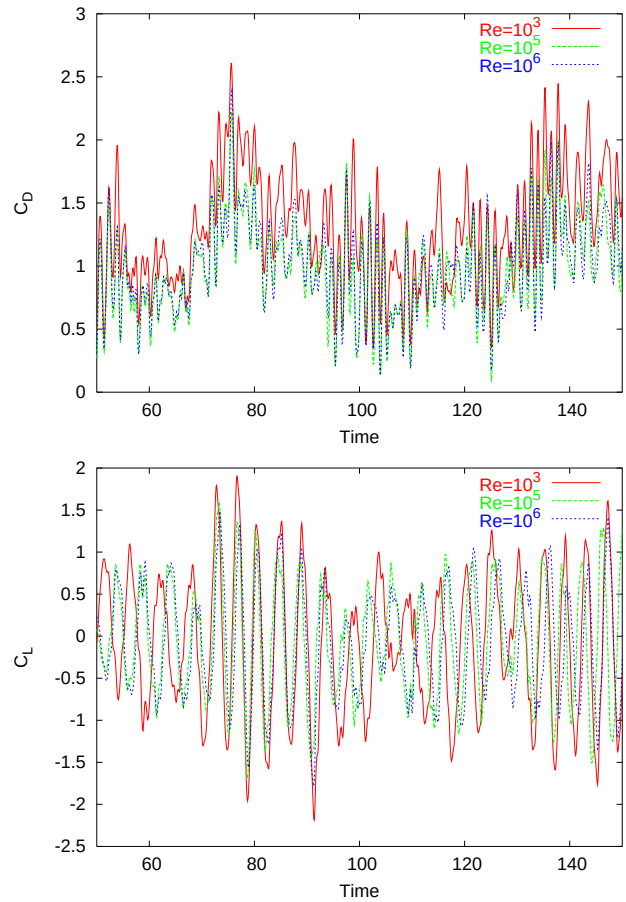

Fig. 17. C_D and C_L responses to the turbulent inflow for a series of higher Reynolds numbers. For trans-critical Reynolds numbers (Re=100,000~1,000,000), a reduction of C_D and C_L amplitudes is observed compared to the sub-critical Reynolds number case (Re=1,000). The same inflow turbulence profile as shown in Fig. 2 is used for three cases.

As shown in Fig. 17, as the Reynolds number falls in the trans-critical regime (Re=100,000~1,000,000), a reduction of the C_D and C_L amplitudes is observed. This seems due to the boundary layer transition from laminar to turbulent, typically accompanying the delayed separation of boundary layer and narrowed wake region. The entire flow field is regarded under the effect of the current turbulence model, and no trip function is used for triggering the boundary layer transition at a desired point. The reduction of drag and lift coefficients for trans-critical regime can be considered purely due to the increased Reynolds number.

Copyright © #### by ASME

The general patterns of the hydrodynamic forces exerted on the cylinder are same as those summarized in the previous section. There is a slight phase shortening observed for the trans-critical Reynolds numbers compared to the Re=1,000 case, and this phase shift may be contributed to the fact that there is slight increase of St as Reynolds number goes higher. However, further investigation is need for this problem.

CONCLUSIONS

The inflow turbulence effect on the hydrodynamic forces exerted on a circular cylinder was investigated by using Reynolds-averaged Navier-Stokes simulations. The range of Reynolds numbers considered was from low sub-critical to supercritical. Time step and mesh resolution studies with various Reynolds numbers were performed for resolution of inflow turbulence. All cases of current profile turbulence were also compared to their corresponding uniform current cases in terms of the amplitudes and frequencies of the forces.

A similar pattern of hydrodynamic forces was observed for the varying Reynolds numbers; namely the higher the inflow turbulence the higher the drag (in-line force), and the time series of the drag coefficient C_D follows the time series of the inflow stream-wise velocity fluctuations. Furthermore, the higher C_D always "accompanies" a higher lift coefficient C_L and faster vortex shedding. Frequency analysis was performed for the time series of the C_L responses. As the inflow condition is changed from uniform to turbulent, extra frequencies of vortex shedding were observed, and even so for the higher Reynolds number cases.

Finally, a reduction of C_D and C_L was observed with Reynolds numbers above 100,000 compared to Re=1,000 case, which seems to be due to the boundary layer transition from laminar to turbulent.

ACKNOWLEDGMENTS

The support of the Offshore Technology Research Center is appreciated. We also thank Dr. R. Mercier for providing the inflow turbulence profiles.

REFERENCES

[1] Mercier, R., 2003, private communication
[2] Chorin, A. J., 1967, "A numerical method for solving incompressible viscous flow problems," Journal of Computational Physics, 2, pp. 12-26
[3] Belov, A., Jameson, A., and Martinelli, L., 1995, "A new implicit algorithm with multigrid for unsteady incompressible flow calculations," AIAA Paper 95-0049
[4] Jameson, A., 1991, "Time dependent calculations using multigrid, with applications to unsteady flows past airfoils and wings," AIAA Paper 91-1596
[5] Pope, S. B., 2000, Turbulent Flows, Cambridge University Press
[6] Kallinderis, Y., 1996, "A 3-D Finite-Volume method for the Navier-Stokes equations with adaptive hybrid grids," Applied Numerical Mathematics, 20, pp. 387-406
[7] Spalart, P. R. and Allmaras, S. R., 1992, "A one-equation turbulence model for aerodynamic flows," AIAA Paper 92-0439

Copyright © #### by ASME